Nanoscale

PAPER

View Article Online
View Journal | View Issue

Cite this: *Nanoscale*, 2022, **14**, 4712

Self-limiting nitrogen/hydrogen plasma radical chemistry in plasma-enhanced atomic layer deposition of cobalt†

Ji Liu, [a] Hongliang Lu, [b] David Wei Zhang[b] and Michael Nolan *[a]

Cobalt (Co) is a potential candidate in replacing copper for interconnects and has been applied in trenches in the semiconductor industry for over twenty years. A non-oxidizing reactant is required in the plasma-enhanced atomic layer deposition (PE-ALD) of thin films of metals to avoid O-contamination. PE-ALD of Co has been demonstrated experimentally with plasma sources of NH_3 or a mixture of N_2 and H_2, but the growth mechanism and key reactions are not clear. In this study, we have investigated the reactions of plasma-generated predominant species, *i.e.* radicals $^{\bullet}H$, $^{\bullet}N$, $^{\bullet}NH$ and $^{\bullet}NH_2$, at metal precursor ($CoCp_2$) treated Co(001) and Co(100) surfaces using static DFT calculations at 0 K and molecular dynamics simulations at 600 K. The proposed reaction mechanisms are (1) $^{\bullet}N$ radicals play an important role in eliminating the surface-bound Cp ligand (if any) *via* pyridine (C_5H_5N) formation and desorption, whereas $^{\bullet}H$ radicals have endothermic reactions for eliminating the Cp ligand *via* CpH formation and desorption; (2) the surface NH_x species are eliminated by $^{\bullet}H$ radicals *via* NH_3 formation and desorption. The simulations of these key reactions show that on the Co(001) surface, the remaining Cp ligand and surface NH_x species after the metal precursor pulse will be completely removed with $^{\bullet}N$ and $^{\bullet}H$ radicals, resulting in Co atoms deposited on the Co(001) surface at a coverage of 3.03 Co nm^{-2}. However, on the Co(100) surface, the surface NH_2 species cannot be completely removed *via* NH_3 formation and desorption due to overall endothermic reactions. Instead, $^{\bullet}H$ radicals react with trench N species, resulting from H transfer in the metal precursor pulse, to form NH. These trench N species cannot be eliminated completely on the Co(100) surface, which will be the source of N impurities in the deposited Co thin films. At the post-plasma stage, the metal surface will be covered with NH_x-terminations with plasma generated $^{\bullet}NH$ radicals and is then ready for the next deposition cycle. Our DFT results highlight and explain why ammonia or H_2/N_2 plasma, which produce NH_x species, are required to deposit high-quality and low-impurity Co thin films using Co metallocene precursors.

Received 24th August 2021,
Accepted 22nd February 2022

DOI: 10.1039/d1nr05568b

rsc.li/nanoscale

1. Introduction

Copper (Cu) has been used in the semiconductor industry as the interconnect material for over 20 years.[1] However, continuous deposition of conducting Cu films in the small and complex structures of the present and future nanoelectronic device structures is, and will become more difficult. Copper requires a liner or seed layer to promote continuous film deposition. This layer is in addition to the barrier layer, which prevents the diffusion of Cu into the dielectric layer and Si substrates.[2] As device dimensions shrink and more complex structures emerge, the volume available for copper interconnects at the transistor levels becomes correspondingly smaller and must accommodate the barrier, the liner and copper.

From a more general perspective, it is well known that at the nanoscale, Cu will preferentially aggregate into high resistivity 3D island structures.[3,4] One solution to these issues is to replace copper with alternative metals that do not suffer from these issues. In this regard, the early transition metal cobalt (Co) is of high interest as an alternative material for replacing Cu in next generation interconnects. Co has already been used in trenches and vias with the downsizing of semiconductor devices.[5–7]

Finding suitable barrier/liner layers and combining these properties into one material is an outstanding challenge because the volume available in trenches and vias exacerbates

[a]*Tyndall National Institute, University College Cork, Lee Maltings, Dyke Parade, Cork, T12 R5CP, Ireland. E-mail: Michael.nolan@tyndall.ie; Tel: +353 021 2346983*
[b]*State Key Laboratory of ASIC and System, Shanghai Institute of Intelligent Electronics & Systems, School of Microelectronics, Fudan University, Shanghai 200433, China*

†Electronic supplementary information (ESI) available. See DOI: 10.1039/d1nr05568b

the issues with copper, so a smaller volume occupied by the barrier and liner layer will help. However, it is clear that copper will ultimately be replaced by another metal.

There is also the question of the deposition of interconnect metals, in particular into high aspect ratio structures in nanodevices, where different surface facets are present and standard physical vapour deposition (PVD) will not give sufficient conformality and uniformity in these structures. Atomic layer deposition (ALD) is widely applied for conformal and uniform deposition, offering a high degree of control over deposition at the atomic level, which is required for metal deposition onto high aspect ratio structures in nanodevices.[8,9] Generally, ALD consists of two self-limiting half cycles, where the reactions will stop after all available surface sites are consumed and repeated cycling through the two half reactions allows a fine level of control over the thickness and conformality of the deposited film. In addition to the successful application of ALD in microelectronics and the semiconductor industry, it is seeing exciting applications in the areas of catalysis and energy conversion and storage.[6,10,11]

For the ALD of Co metal, cyclopentadienyl (Cp) based precursors such as the $CoCp_2$ metallocene, $CoCp(CO)_2$ and Co (CpAMD) have been used in thermal and plasma-enhanced ALD.[12,13] For thermal ALD of Co with metal acetamidinates and hydrogen, the required growth temperature can be as high as 350 °C, while the growth rate can be as low as 0.12 Å per cycle.[14] With the application of plasma-enhanced ALD (PE-ALD) using NH_3 plasma, the Co PE-ALD process window is between 200 °C and 250 °C, with a reported growth rate of 0.5 Å per cycle.[15] The reported growth per cycle with dicobalt octacarbonyl ($Co_2(CO)_8$) and H_2 plasma is increased to 1.2 Å per cycle in the ALD window of 75 °C to 110 °C.[16] The Co metal precursor $CoCp(CO)_2$ has an even larger reported GPC at 1.5 Å per cycle using NH_3 plasma at a higher temperature of 300 °C.[17]

The reaction mechanism of film growth with ALD using an oxidizing reactant such as O_3 and H_2O is well-established.[18–21] However, when depositing metals, an O-source will promote oxidation of the metal and therefore cause contamination and severely modify the properties of the metal. To address this issue, non-oxidizing reactants such as NH_3 have been used in PE-ALD of transition metals such as Ta, Ti, Ru and Co.[22–25] For the plasma source, a mixture of N_2 and H_2 is used and the properties of the deposited metal thin film largely depend on the N_2/H_2 gas flow ratio.[23,26] It has been observed that a H_2 plasma alone or separate N_2 and H_2 plasmas result in high resistivity and low purity Co thin films.[27] Previous studies argue that the presence of NH_x species is needed to deposit low resistivity and high purity Co thin films.[27] These NH_x species are proposed to promote the chemisorption of the metal precursor and the removal of the Cp ligand, analogous to the role of hydroxyl groups in metal oxide ALD.[20,21,28,29] But they are not incorporated in the film, because N may desorb in the form of either NH_3 or N_2.

The incorporation of nitrogen into a PE-ALD deposited Co film is temperature-dependent. The formation of CoN_x was reported during the deposition of Co thin films using $CoCp_2$ and NH_3 plasma at temperatures below 300 °C.[30] For deposition temperatures above 350 °C, decomposition of CoN_x was effectively complete, resulting in pure Co thin films.[30] The detailed mechanism of plasma assisted metal deposition has not yet been established and requires deeper investigations. A plausible proposal is that highly reactive radicals from the hydrogen/nitrogen-plasma source must be present for successful PE-ALD of metals.

A complete PE-ALD process using N-plasma (NH_3 or a mixture of N_2 and H_2)[27] can be thought to follow the following process (Scheme 1): firstly, it is vital to note that at the post-plasma stage, the metal surface is actually an NH_x-terminated metal surface, where $x = 1$ or 2.[31] In the metal half-cycle, the metal precursor $CoCp_2$ reacts with the NH_x-terminated metal surface. Cp ligands are eliminated by hydrogen transfer from the surface to form CpH, which desorbs from the surface, rather than migrating to another Co site on the surface.[32] In the second half-cycle, the plasma-generated radicals such as N_xH_y ($x = 0, 1$; $y = 0, 1, 2$) will react with the precursor fragment-terminated metal surface, eliminating any remaining metal ligands from the surface, and covering the metal surface in some concentration of NH_x groups at the end of the second half cycle.

In our recent published work, the nature and stability of NH_x-terminated Co(001) and Co(100) surfaces and the structures after the metal precursor $CoCp_2$ pulse were studied.[31,32] The results show that under typical ALD operating conditions from the literature[5] (temperature range 550 K to 650 K), the most stable termination of the low energy Co(001) surface is 0.56 ML coverage of NH-termination. On the high energy, zigzag Co(100) surface, a mixture of 0.67 ML NH and 0.67 ML NH_2 is the most stable surface termination. With these NH_x terminations, on the Co(100) surface, the metal precursor can undergo two hydrogen transfer steps and the two Cp ligands are eliminated completely, resulting in Co atom deposition on the surface whereby Co binds to the N atom. However, on the Co(001) surface, only one Cp ligand is eliminated, resulting in CoCp fragments on the surface after the metal precursor pulse. The computed surface coverage of the final terminations after the metal precursor pulse is 3.03 CoCp nm^{-2} on the NH_x-terminated Co(001) surface and 3.33 Co nm^{-2} on the NH_x-terminated Co(100) surface.[32]

During the plasma cycle, the active plasma species can include radical species ($^{\bullet}H$, $^{\bullet}N$, $^{\bullet}NH$, and $^{\bullet}NH_2$) and ions produced by electron-induced ionization of neutrals (such as H^+, N^+, H_2^+, and NH_3^+). Sode[33] *et al.* studied and modelled the density of these active plasma species and found out that the density of radicals (*ca.* 10^{18} m^{-3}) is much larger than the density of ions (*ca.* 10^{14}–10^{16} m^{-3}). Therefore, to make the calculations in this study tractable, we assume that plasma generated radicals $^{\bullet}H$, $^{\bullet}N$, $^{\bullet}NH$, and $^{\bullet}NH_2$ are the predominant active species. In the work of Shimizu[34] *et al.*, the quantities of incoming radical species arriving at the substrate surface decease in the order $^{\bullet}H > {}^{\bullet}NH_2 > H_2$, $N_2 > N_2H_2 > {}^{\bullet}NH > N_2H_4$. Based on these studies, we considered it reasonable to

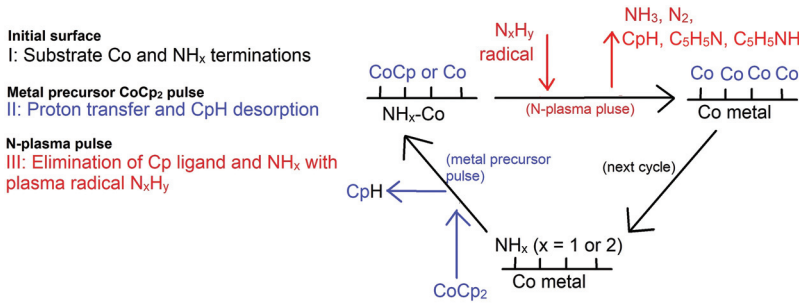

Scheme 1 Illustration of PE-ALD of Co using $CoCp_2$ and NH_3 or N_2/H_2 plasma.

consider the plasma-generated radicals $^{\bullet}NH_2$, $^{\bullet}NH$, $^{\bullet}H$ and $^{\bullet}N$ in our work. Simulating charged species within the three dimensional periodic boundary conditions in a periodic plane wave basis code such as VASP is problematic and the energies resulting from such calculations are not reliable, so this prevents us from including such species in the calculation.

The reactions of plasma generated radicals $^{\bullet}H$, $^{\bullet}N$, $^{\bullet}NH$, and $^{\bullet}NH_2$ with the metal precursor treated Co(001) and Co(100) surfaces were investigated in detail with density functional theory (DFT) calculations. We use static DFT relaxations at 0 K and *ab initio* molecular dynamics simulations at 600 K to explore the chemistry of these radicals and how they remove Cp ligands and NH_x species and recover the NH_x terminations needed to promote the metal precursor step.

We find that $^{\bullet}N$ radicals play an important role in eliminating surface bound Cp ligands on the Co(001) surface *via* pyridine formation and desorption and $^{\bullet}H$ radicals can promote the elimination of NH_x species on the Co(001) surface *via* NH_3 formation and desorption. These reactions are overall exothermic, and the surface Cp ligand and NH_x species can be removed completely from the Co(001) surface, resulting in deposited Co atoms on the Co(001) surface at a coverage of 3.03 Co nm^{-2}. Furthermore, plasma-generated NH_x species can then cover the Co(001) surface by reacting with the deposited Co atoms to make new Co–N bonds.

However, on the Co(100) surface, the surface NH_2 species cannot be fully removed *via* NH_3 formation and desorption due to an overall endothermic reaction pathway. $^{\bullet}H$ radicals contribute to transforming the N species in the Co(100) trench sites to NH. This study shows that these N species are potential sources of N impurities in Co thin film deposition with PE-ALD due to the high energy cost of eliminating these N species.

These findings confirm that plasma radicals play a crucial role in adsorbing metal precursor $CoCp_2$ with the formation of NH_x-terminations on metal surfaces, and the elimination of any remaining Cp ligands that cannot be completely removed during the metal precursor pulse. For Cp-based metal precursors, NH_x species are required to deposit Co thin films with high purity and low resistivity, which explains why NH_3 plasma or a mixture of N_2 and H_2 plasma are the most favourable sources for Co deposition, rather than H_2 plasma or N_2 plasma alone.

2. Methods and computational details

All the calculations are performed on the basis of periodic spin-polarized density functional theory (DFT) within a plane wave basis set and projector augmented wave (PAW) formalism,[35] as implemented in the Vienna *ab initio* simulation package (VASP 5.4) code.[36] The generalized gradient approximation (GGA) with the parameterization 'of Perdew–Burke–Ernzerhof (PBE) is used for the exchange–correlation functional.[37,38] We use 9 valence electrons for Co, 5 for N, 4 for C, and 1 for H. The plane wave energy cut-off is 400 eV. The convergence of energy and forces are set at 1×10^{-4} eV and 0.01 eV $Å^{-1}$, respectively. The bulk Co crystal structure is optimized by simultaneously relaxing the ionic positions, cell volume and cell shape at a higher plane wave energy cut-off of 550 eV and using a Monkhorst–Pack grid *k*-point mesh[39] of 12 × 12 × 6. The resulting lattice constants are $a = b = 2.49$ Å, and $c = 4.03$ Å. This c/a ratio at the value of 1.62 is in good agreement with previous studies.[40]

The deposited Co films by PE-ALD are polycrystalline and have random surface orientations after low-temperature deposition. Based on our previous study[31] on the stability of NH/NH_2 terminations of Co surfaces, we have chosen the most stable Co(001) surface (with the lowest surface energy) and to assess the role of surface structure and reactivity, we also consider the Co(100) surface, which has a higher surface energy but high reactivity in our investigation of the precursor reaction mechanisms. A similar comparison has been presented for copper.[41] Other surface facets, such as Co(110) and Co(101) would be interesting for future study. A (4 × 4) supercell is used to model the (001) surface with a surface lattice of $a = b =$ 9.96 Å (surface area = 0.99 nm^2) while a (3 × 3) supercell, with a surface lattice of $a = 7.47$ Å, $b = 12.10$ Å (surface area = 0.90 nm^2), is used to model the (100) surface. For the Co(001) surface, a five-layer slab is used, with the bottom three layers fixed during the calculation; however for the Co(100) surface, due to its zigzag structure, a four-bilayer (eight-atomic-layer) slab is built with the bottom two bilayers (bottom four layers) fixed during the calculations. From our previous studies, fixing these layers is sufficient to model these Co surfaces.[31] A *k*-point mesh[39] of 2 × 2 × 1 is used in the (4 × 4) supercell, and for the (3 × 3) supercell a 3 × 2 × 1 mesh is used. The van der

Waals correction was applied with the PBE-D3 method to ensure an accurate description of the dispersion interactions in the computed adsorption energies.[41] Charge transfer is analysed with the Bader charge analysis procedure.[42,43] This was computed from the difference between the Bader charge and the number of valence electrons.

From our previous study, after the metal precursor ($CoCp_2$) pulse, the surface terminations are CoCp fragments on NH_x-terminated Co(001) surface at a coverage of 3.03 CoCp nm^{-2} and deposited Co atoms on NH_x-terminated Co(100) surface at a coverage of 3.33 Co nm^{-2}. These configurations after the metal precursor pulse are shown in Fig. 1. On the Co(100) surface, mixed NH_x terminations with NH occupying trench sites and NH_2 occupying surface sites are determined.[31] Trench NH species contribute to eliminating Cp ligands during the metal precursor pulse, resulting in bare N atoms on trench sites (Fig. 1(b)).

This work investigated the reaction mechanism, key reaction steps, and key by-products by modelling the reaction of plasma-generated predominant species, *i.e.* plasma radicals $^{\bullet}H$, $^{\bullet}N$, $^{\bullet}NH$, and $^{\bullet}NH_2$, on metal precursor $CoCp_2$ treated NH_x-terminated Co(001) and Co(100) surfaces. The main contributions are (1) how the surface bound Cp ligands (if any) and surface NH_x species are eliminated with these plasma radicals, and (2) how the metal surfaces are recovered with NH_x-terminations with these plasma radicals to be ready for the next deposition cycle.

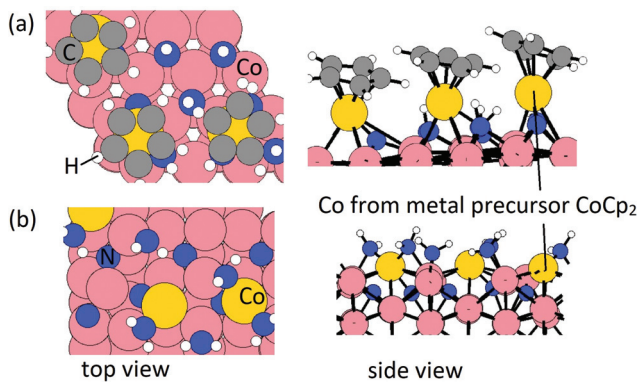

Fig. 1 The configurations of final structures on Co (a) (001) and (b) (100) surfaces after the metal precursor pulse. Carbon, nitrogen, and hydrogen atoms are presented in grey, blue, and white colours. Substrates Co and Co from $CoCp_2$ are represented by pink and yellow spheres, respectively.

3. Results and discussion

3.1 Analysis of reaction schemes

3.1.1 Reaction of plasma radicals on 3CoCp fragment-terminated Co(001) surface. After the metal precursor pulse, the surface termination is the $(CoCp)_3NH_x$-terminated Co(001) surface.[32] We first addressed the interaction of one kind of plasma radical species on this 3CoCp fragment-terminated Co (001) surface and computed the reaction energies of each by-product resulting from plasma radicals reacting with surface CoCp fragments and surface NH_x terminations. The coverage of plasma radicals is one plasma radical per CoCp fragment, so at the highest stable coverage of CoCp fragments at 3.03 CoCp nm^{-2}, we consider 3 $^{\bullet}H$, 3 $^{\bullet}N$, and 3 $^{\bullet}NH$, respectively. These results are summarized in Table 1.

The reaction energies per plasma radical are calculated by

$$\Delta E = (E_{total} - E_{sub} - 3 \times E_{plasma})/3 \quad (1)$$

where E_{total} and E_{sub} are the energies of plasma radicals treated $(CoCp)_3NH_x$-terminated Co(001) surface and the $(CoCp)_3NH_x$-terminated Co(001) surface, respectively. E_{plasma} is the energies of plasma-generated radicals, *i.e.* $^{\bullet}H$, $^{\bullet}N$, $^{\bullet}NH$, and $^{\bullet}NH_2$. In this study, $^{\bullet}H$ and $^{\bullet}N$ radicals are referenced to half of H_2 and N_2, while $^{\bullet}NH$ or $^{\bullet}NH_2$ radicals are referenced to $\frac{1}{2}(N_2 + H_2)$ or $(\frac{1}{2}N_2 + H_2)$, respectively, which is consistent with our previous thermodynamic study of NH_x terminations.[31]

Elimination of Cp ligand via CpH formation and desorption. One hydrogen radical is placed near each Cp ring with an initial C–H distance of 1.9 Å. The initial structure and relaxed stable structure are shown in Fig. 2. After relaxing, 3 CpH are formed spontaneously, with an energy change of 0.03 eV per Cp and C–H bond distance of 1.1 Å. The computed energy cost per CpH for the CpH desorption process, which results in three Co atoms deposited on the Co(001) surface, is 1.29 eV per Cp. The removal of Cp ligand on $(CoCp)_3NH_x$-terminated Co(001) surface *via* CpH formation and desorption is overall endothermic with an energy cost of 1.32 eV per Cp. This is significantly reduced compared with the high energy cost of CpH formation and desorption on one CoCp fragment-terminated Co(001) surface (4.70 eV per CpH, Table S1 in the ESI†) and

Table 1 Summary of reactions of surface species, *i.e.* Cp ligand and NH_x species, and plasma radicals H, N, and NH on CoCp fragments on an NH_x-terminated Co(001) surface at the coverage of 3.03 CoCp nm^{-2}. The coverage of plasma radicals is one plasma radical per CoCp fragment, and is 3 $^{\bullet}H$, 3 $^{\bullet}N$, and 3 $^{\bullet}NH$. The by-products are formed spontaneously after structure relaxing

Surface species	Plasma radicals	By-product	Energy changes upon by-product formation per by-product	Desorption energy per by-product
3 Cp	3 $^{\bullet}H$	3 CpH (C_5H_6)	0.03 eV per CpH	1.29 eV per CpH
	3 $^{\bullet}N$	3 Pyridine (C_5H_5N)	−2.23 eV per pyridine	1.17 eV per pyridine
	3 $^{\bullet}NH$	3 Pyridinium (C_5H_5NH)	−2.62 eV per pyridinium	2.25 eV per pyridinium
3 NH	3 $^{\bullet}H$	3 NH_2	−0.10 eV per NH_2	—
3 NH_2	3 $^{\bullet}H$	3 NH_3	−1.05 eV per NH_3	1.01 eV per NH_3

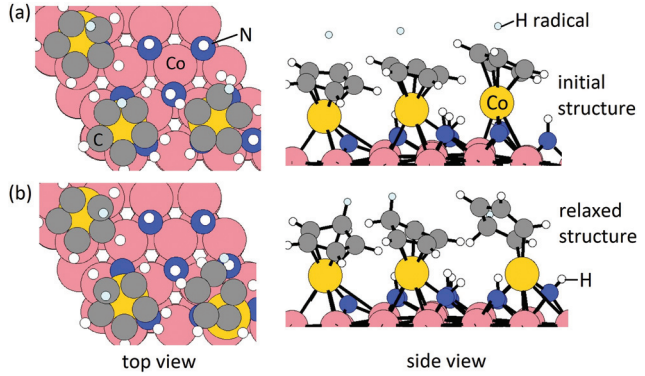

Fig. 2 Configurations of top view and side view of (a) initial structure, and (b) relaxed structure for reactions of H radical and Cp ligand on NH_x-terminated Co(001) surface at the coverage of 3.03 CoCp nm^{-2}. Carbon, nitrogen, and hydrogen atoms are presented in grey, blue, and white colours. H radicals are represented by a light blue sphere. Substrates Co and Co from $CoCp_2$ are represented by pink and yellow spheres, respectively.

indicates a cooperative role of the surface-bound CoCp species in promoting ligand elimination at this higher coverage of CoCp fragments. This cooperative effect means that once sufficient numbers of precursor fragments/molecules are present on the metal surface, it can show enhanced activity for ligand exchange and desorption with lower energy cost, which is analogous to cooperative mechanism on proton transfer and ligand desorption for ALD of metal oxide such as Al_2O_3 and HfO_2.[44]

Elimination of Cp ligand via pyridine formation and desorption. For the formation of pyridine or pyridinium cation, one $^{\bullet}N$ or $^{\bullet}NH$ radical is allowed to insert into a C= bond in each Cp ligand. The configurations of relaxed structures are shown in Fig. 3. The energy change upon N or NH insertion is −2.23 eV per Cp and −2.62 eV per Cp, respectively. The computed

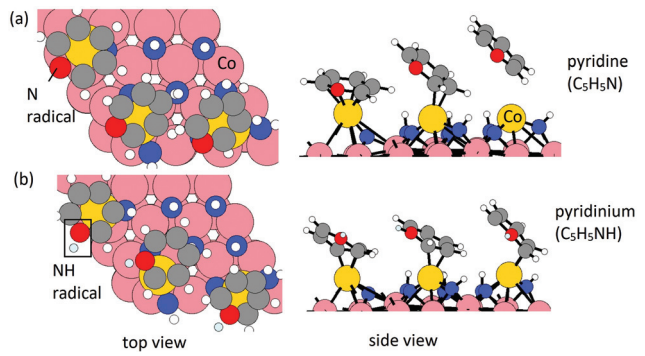

Fig. 3 Configurations of top view and side view of (a) C_5H_5N, (b) C_5H_5NH for the insertion of plasma radicals N or NH into a C= bond of the Cp ligand on NH_x-terminated Co(001) surface at the coverage of 3.03 CoCp nm^{-2}. Carbon, nitrogen, and hydrogen atoms are presented in grey, blue, and white colours. Substrates Co and Co from $CoCp_2$ are represented by pink and yellow spheres, respectively. Plasma-generated N and H radicals are represented by red and light blue spheres, respectively.

energy cost per pyridine or pyridinium for the desorption process, resulting in three Co atoms deposited on the (001) surface, is 1.17 eV per pyridine and 2.25 eV per pyridinium, respectively. The removal of Cp ligand on $(CoCp)_3NH_x$-terminated Co(001) surface *via* pyridine or pyridinium formation and desorption is overall exothermic with an energy gain of −1.06 eV per pyridine and −0.37 eV per pyridinium. For the lower CoCp coverage of one CoCp fragment, the computed energy cost of CpH formation and desorption is at the value of 2.32 eV per pyridine and 3.00 eV per pyridinium (Table S1 in the ESI†), which is a high energy cost and an overall endothermic reaction at this lower CoCp coverage. We see a cooperative role of the surface-bound CoCp species in promoting ligand elimination *via* pyridine formation and desorption at higher CoCp coverage, which is analogous to Cp ligand elimination *via* CpH formation and desorption.

Overall, the Cp ligand elimination *via* pyridine or pyridinium formation and desorption are exothermic at the $(CoCp)_3NH_x$-terminated Co(001) surface, whereas it is overall endothermic for Cp ligand elimination *via* CpH formation and desorption. Thus, the predicted primary product of eliminating the Cp ligand is pyridine (C_5H_5N), which is the same as the case of lower CoCp coverage as analysed in the ESI.†

Elimination of surface NH_x species with the presence of Cp ligand. To investigate the interaction with the surface NH_x species, 3 $^{\bullet}H$ radicals are placed near three surface NH species with initial H–N distances at 1.5 Å and CoCp fragments are present on the surface. The reaction energies are computed by

$$\Delta E = E_{\text{total}} - E_{\text{sub}} - n \times E_{\text{H}} + m \times E_{\text{NH}_3} \quad (2)$$

where E_{total} and E_{sub} are the energies of plasma $^{\bullet}H$ radical-treated, $(CoCp)_3NH_x$-terminated Co(001) surface and the $(CoCp)_3NH_x$-terminated Co(001) surface, respectively. E_{H} is the energy of plasma-generated $^{\bullet}H$ radicals, which is referenced to half of H_2. E_{NH_3} is the energy of NH_3 that desorbs from the metal surface. The number of $^{\bullet}H$ radicals and NH_3 are indicated by n and m, respectively.

The configurations of initial and relaxed stable structures of intermediate NH_2 formation are shown in Fig. 4. After the formation of intermediate NH_2, with a computed negative reaction energy of −0.10 eV per NH_2 and N–H bond distance of 1.0 Å, 3 additional $^{\bullet}H$ radicals are then positioned near these surface NH_2 species. After relaxing, NH_3 forms spontaneously as shown in Fig. 5, with an energy gain of −1.05 eV per NH_3. The computed energy cost per NH_3 for the desorption process is 1.01 eV per NH_3, but this is more than offset by the exothermicity of the NH and NH_2 formation steps. Thus, the elimination of surface NH species *via* NH_3 formation and desorption with the presence of Cp ligand is overall slightly exothermic with an energy gain of −0.14 eV per NH_3.

Elimination of surface NH_x species with initial Cp ligand removal. We now consider the elimination of surface NH_x on the $(CoCp)_3NH_x$-terminated Co(001) surface using $^{\bullet}H$ radicals, in which the Cp ligand was removed in the first step *via*

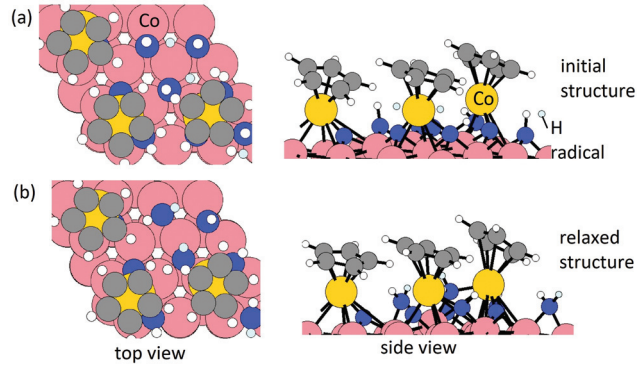

Fig. 4 Configurations of top view and side view of (a) initial and (b) relaxed structure for intermediate NH_2 formation with H radical. Carbon, nitrogen, and hydrogen atoms are presented in grey, blue, and white colours. H radicals are represented by light blue spheres. Substrates Co and Co from $CoCp_2$ are represented by pink and yellow spheres, respectively.

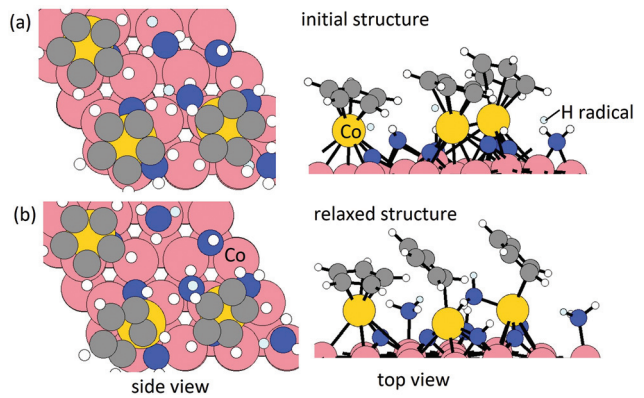

Fig. 5 Configurations of top view and side view of (a) initial and (b) relaxed structure for ammonia formation with H radical and intermediate NH_2. Carbon, nitrogen, and hydrogen atoms are presented in grey, blue, and white colours. H radicals are represented by light blue spheres. Substrates Co and Co from $CoCp_2$ are represented by orange and yellow spheres, respectively.

pyridine formation and desorption. The reaction energies are computed by

$$\Delta E = E_{\text{total}} - E_{\text{sub}} - n \times E_{\text{H}} + m \times E_{\text{NH}_3} + 3 \times E_{\text{pyridine}} \quad (3)$$

where E_{total} and E_{sub} are the energies of plasma $^{\bullet}$H radical treated $(CoCp)_3NH_x$-terminated Co(001) surface and the $(CoCp)_3NH_x$-terminated Co(001) surface, respectively. E_{H} is the energy of plasma generated $^{\bullet}$H radical, which is referenced to half of H_2. E_{NH_3} is the energy of NH_3 that desorbs from metal surface. E_{pyridine} is the energy of free pyridine. The number of $^{\bullet}$H radicals and NH_3 are indicated by n and m, respectively.

The plotted reaction pathway and configurations of structures along the pathway are shown in Fig. 6 and Fig. S9,† respectively. The computed reaction energies for initial Cp ligand removal and subsequent ammonia formation are all negative on the $(CoCp)_3NH_x$-terminated Co(001) surface. A cooperative effect of the surface-bound CoCp fragments is observed when compared to a single CoCp fragment (Fig. S3 in the ESI†), which makes the removal of the Cp ligand exothermic and favourable on the surface with the highest CoCp coverage. For the removal of surface NH species, the determined preferred pathway is an exothermic NH → NH_2 → NH_3. After the Cp ligand and NH_x species are removed completely, three Co atoms are deposited on the Co(001) surface, with a computed exothermic reaction energy of −4.85 eV.

The plotted reaction energies for the case that Cp is first eliminated as CpH is shown in Fig. S10.† We see that the computed reaction energies of CpH and NH_3 formation and desorption are all positive and the reactions are endothermic, compared to overall exothermic reactions *via* Cp eliminated as pyridine. We would expect that pyridine is a primary product from eliminating the Cp ligand during the plasma cycle.

To summarize, these T = 0 K results indicate that the $^{\bullet}$N radical plays an important role in eliminating Cp ligands present on the surface (if any) *via* pyridine formation and desorption and $^{\bullet}$H radicals contribute to the elimination of surface NH_x species *via* NH_3 formation and desorption, where the surface Cp ligands are removed prior to the elimination of these surface NH_x species.

Our calculations show that on the Co(001) surface, the energetically preferred mechanism is that the Cp ligand is eliminated prior to surface NH_x species *via* pyridine formation and desorption with plasma-generated N radicals. The computed reaction energies are overall exothermic. While in the previous experimental studies, there was no explicit discussion of potential pyridine elimination, M. F. J. Vos[27] *et al.* do mention that N-containing products are possible. It would be interesting to explore the by-products of plasma chemistry using Fourier transform infrared (FTIR) and/or quadrupole mass spectroscopy (QMS) analysis.

The elimination process of surface NH species is exothermic when using $^{\bullet}$H radicals. NH species are removed *via* intermediate NH_2 formation, by-product NH_3 formation and desorption. Surface N species, resulting from H transfer to Cp ligand on metal precursor pulse, are also removed *via* NH, NH_2 formation, and release of NH_3. The surface NH_x species are completely eliminated with plasma-generated H radicals, resulting in the deposition of Co atoms on the Co(001) surface at a coverage of 3.03 Co nm^{-2}.

3.1.2 Reactions of plasma radicals on the NH_x-terminated Co(100) surface. After the metal precursor ($CoCp_2$) pulse, the higher surface energy Co(100) surface is terminated with Co atoms at a coverage of 3.33 Co nm^{-2}. From our previous study[32] on the mechanism of metal precursor pulse, the trench NH species are involved in the H transfer to eliminate the Cp ligand as CpH. The surface NH_2 species have endothermic reaction energies for CpH elimination. Thus, after the metal precursor pulse in a (3 × 3) supercell, we have three deposited Co atoms with six surface NH_2 and six trench N atoms that have lost H atoms in the metal precursor step (Fig. 1(b)).

During the plasma step, these remaining NH_x species may be eliminated by the reaction with plasma-generated radicals

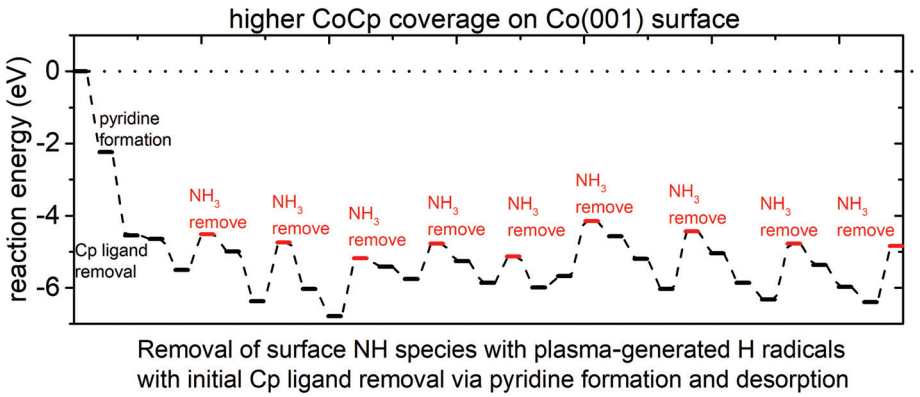

Fig. 6 The plotted reaction pathway for removal of surface NH species with plasma generated H radicals with initial Cp ligand removed from 3CoCp-terminated Co(001) surface. The steps of H radical addition are indicated by the black markers and the steps of NH_3 desorption are indicated by the red markers. The Cp ligand is first eliminated as pyridine.

$^{\bullet}H$, $^{\bullet}N$, $^{\bullet}NH$, and $^{\bullet}NH_2$ *via* NH_3, N_2H_2, or N_2H_4 formation and desorption, analogous to the removal of surface NH_x species on the Co(001) surface.

Elimination of surface NH_2 species. We first performed calculations for reactions of eliminating surface NH_2 species with $^{\bullet}H$ radicals *via* NH_3 formation and desorption. The $^{\bullet}H$ radicals are placed near the surface NH_2 with an initial N–H distance of 1.5 Å and the successive interactions of the surface NH_2 are examined. The plotted energy pathway for ammonia formation and desorption is shown in Fig. 7.

The reaction energies are computed by eqn (2) as defined above. The configurations of structures along the reaction pathway are shown in Fig. S11.† While ammonia is formed spontaneously after relaxing the structure, the computed reaction energies are all positive, indicating endothermic reactions for the removal of surface NH_2 species with $^{\bullet}H$ radicals. The energy cost of NH_3 desorption on Co(100) surface is around 1.2 eV at each desorption step. After the desorption of the 6th NH_3, the overall reaction energy is as high as 5.80 eV. This indicates that on NH_x-terminated Co(100) surface, the surface NH_2 species cannot be completely eliminated by $^{\bullet}H$ radicals.

Elimination of trench N species. We then performed calculations for reactions of trench N species and $^{\bullet}H$ radicals. The results show that trench N species can react with $^{\bullet}H$ radicals to form NH, with a computed reaction energy of 0.24 eV for the 1st NH formation and overall exothermic reaction energy for the following NH formation. However, there are no further reactions to form intermediate NH_2 or by-product NH_3. Instead, the next $^{\bullet}H$ radicals prefer to react with another trench N species to form NH. The plotted reaction pathway for trench NH formation is shown in Fig. 8. The computed reaction energies are overall negative, except for a small energy cost for the formation of the first NH. The configurations of structures along the reaction pathway are shown in Fig. S12.† We note that for the 6th $^{\bullet}H$ radical, it would prefer to bind to surface Co atoms rather than recover the 6th N to NH species. Thus, for the trench N species, at the plasma step with $^{\bullet}H$ radicals, at the most five N species can recover to NH. These results indicate the difficulty in eliminating N species from the Co(100) surface *via* ammonia formation.

Given the difficulty in eliminating surface NH_2 and trench N *via* NH_3 formation and desorption, we have computed the reaction energies for the formation of hydrazine (N_2H_4) and diazene (N_2H_2) that are formed through the interaction with NH and NH_2 radicals. After static DFT relaxations, hydrazine or diazene dissociate into two NH_2 or two NH that are bound

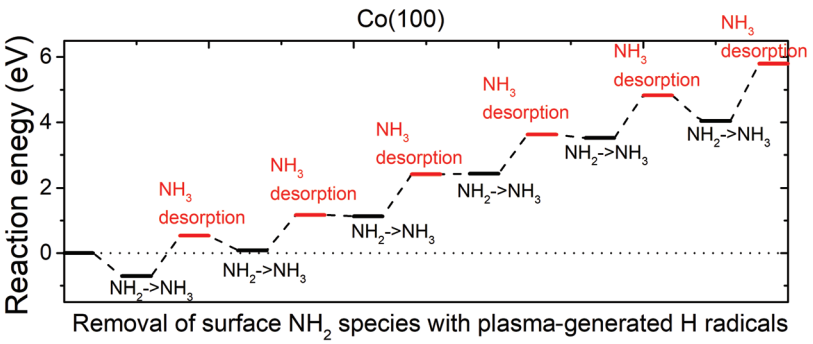

Fig. 7 The plotted reaction pathway for the removal of surface NH_2 species with plasma-generated H radicals on an NH_x-terminated Co(100) surface.

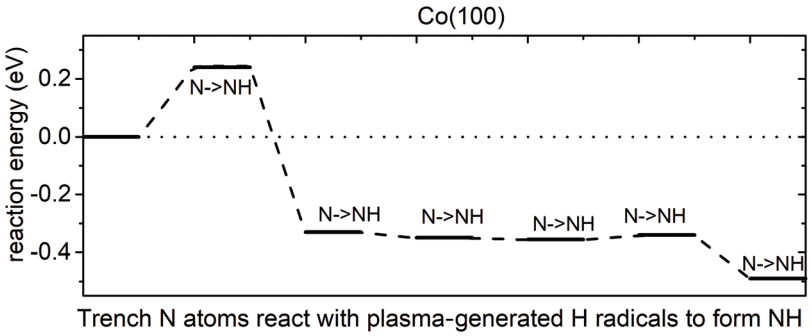

Fig. 8 The plotted reaction pathway for trench N atoms recovered to NH with plasma-generated H radicals on an NH_x-terminated Co(100) surface.

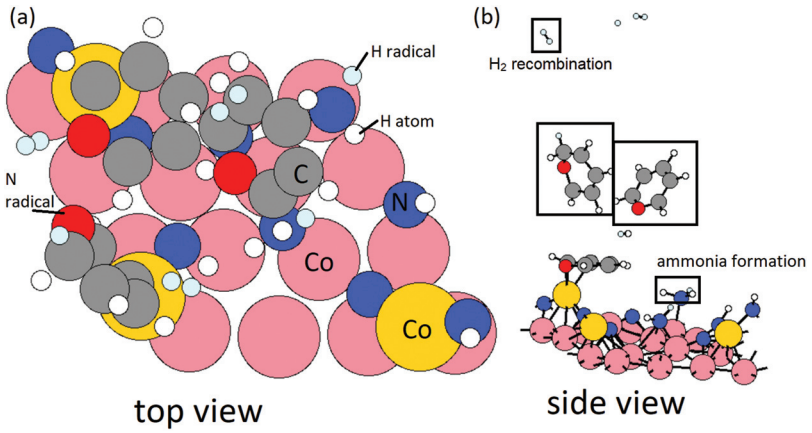

Fig. 9 The structure snapshot at the end of the MD calculation at 600 K on the NH_x-terminated Co(001) surface with 9 H radicals in (a) top view, and (b) side view. Carbon, nitrogen, and hydrogen atoms are presented in grey, blue, and white colours. H radicals are represented by light blue spheres. Substrates Co and Co from $CoCp_2$ are represented by pink and yellow spheres, respectively. H and N radicals are represented by light blue and red spheres, respectively.

to the Co(100) surface, indicating the unfavourable formation of hydrazine and diazene.

To summarise, on the Co(100) surface, the removal of surface NH_x species as ammonia is endothermic, while it is an exothermic reaction on the Co(001) surface. Instead, on Co (100), plasma generated $^{\bullet}H$ radicals react with trench N species to form stable NH species, which are then available for the next hydrogen transfer step in the next metal precursor pulse. Our static DFT calculations at zero K indicates that there is a high energy cost to remove surface NH_x species as ammonia on Co(100) surface with introducing successive plasma generated $^{\bullet}H$ radicals. Thermodynamic analysis is needed to reveal the distinct reaction mechanisms on Co(001) and Co(100) surfaces.

3.2 Thermodynamic analysis of reaction schemes

3.2.1 *Ab initio* molecular dynamics simulations at the $(CoCp)_3NH_x$-terminated Co(001) surface. On the Co(001) surface, *ab initio* molecular dynamics (AIMD) calculations were performed by introducing 9 $^{\bullet}H$ radicals at a temperature of 600 K. We formed pyridine through N radical insertion, at a coverage of 3.03 pyridine per nm^2. The time step was 1.5 fs, with a total running time at 2.25 ps with the NVT (canonical) ensemble. The structures at the end of the MD simulations are shown in Fig. 9 and a movie of the simulation is shown in the ESI.† We see some H recombination in the 9 $^{\bullet}H$ situation, which is first observed at 0.21 ps (Fig. S13(a)†). This is consistent with experimental studies of plasma-assisted deposition of Co.[34] Some $^{\bullet}H$ radicals contribute to NH_3 formation at 0.33 ps (Fig. S13(b)†) and pyridinium formation at 1.26 ps (Fig. S13(c)†). Thus, upon introducing 9 $^{\bullet}H$ radicals on the Co (001) surface with surface-bound pyridine at a coverage of 3.03 pyridine per nm^2, the MD results indicate that surface NH_x species can be eliminated *via* NH_3 formation and desorption while surface-bound pyridine is eliminated *via* either direct desorption or pyridinium formation and desorption. These results are consistent with the static DFT calculations of kinetic analysis of reaction schemes discussed in section 3.1.

3.2.2 *Ab initio* molecular dynamics simulations at the NH_x-terminated Co(100) surface. To explore the dynamics on the Co(100) surface, MD calculations were performed on the NH_x-terminated Co(100) surface with six deposited Co atoms on the surface at temperatures of 600 K and 1000 K. The time step is 1.5 fs with total simulation time of 2.25 ps with the NVT

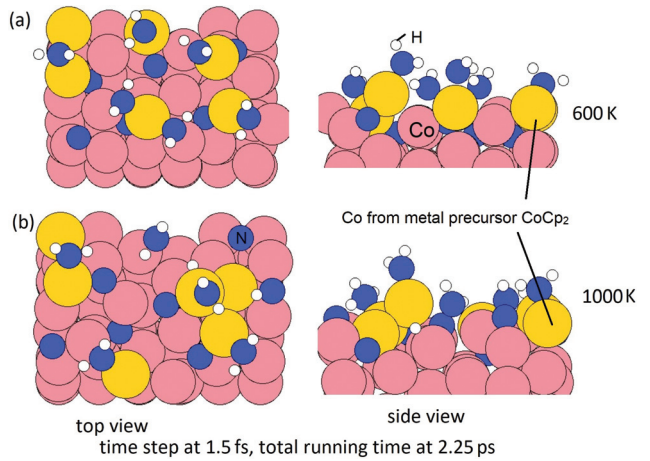

Fig. 10 The configurations of resulting structures after MD calculations at (a) 600 K, and (b) 1000 K on an NH_x-terminated Co(100) surface with six deposited Co atoms on the surface. Carbon, nitrogen, and hydrogen atoms are presented in grey, blue, and white colours. Substrates Co and Co from $CoCp_2$ are represented by pink and red spheres, respectively.

ensemble. The structures at the end of this MD simulation are shown in Fig. 10. For T = 600 K and 1000 K, there is no desorption of surface NH_x terminations indicating that the removal of these surface-bound NH_x species requires a high energy cost. This is in line with the static DFT results of computed endothermic reactions of eliminating surface NH_x species with H radicals. For T = 1000 K, we see that the deposited surface Co atoms migrates to form small Co nanoclusters due to trench N migrating to surface sites.

4. Discussion

4.1 Structures of N-plasma treated Co(001) and Co(100) surfaces

On the low energy Co(001) surface, during the plasma cycle the Cp ligand and surface NH_x species are eliminated by the plasma-generated $^{\bullet}$N and $^{\bullet}$H radicals, resulting in Co atoms being deposited on the Co(001) surface at a coverage of 3.03 Co nm^{-2}. On the Co(100) surface, the surface NH_2 species cannot be eliminated with $^{\bullet}$H radicals since these reactions are endothermic. The trench N species will transform to NH after interaction with $^{\bullet}$H radicals. These trench N species on Co (100) surface will be a potential source of N impurities in deposited Co thin films.[30,45]

We applied Bader charge analysis to the Co(001) and Co (100) surfaces in each step of NH_x removal. The results are summarized in Table 2. On the Co(001) surface, the Cp ligands have been removed prior to the interaction of surface NH species with N radicals. The computed transferred charges for the formation of the ammonia by-product are almost the same at a value of *ca.* $-0.10e^-$ on the NH_x-terminated Co(001) surface. However, on the NH_x-terminated Co(100) surface, the computed transferred charge from NH_3 to the substrate Co atoms in the NH_3 formation step increases from $0.06e^-$ to $0.13e^-$ along the elimination pathway. This indicates that the interaction between NH_3 and substrate Co atoms becomes stronger along the elimination pathway on the Co(100) surface, which is in accordance with the computed positive reaction energies for NH_3 formation and desorption on (100) surface.

On the Co(001) surface, after a few cycles, a full layer of Co atoms will be deposited on the surface, and the surface NH_x species are completely removed at the plasma cycle. However, on the Co(100) surface, the NH_x species cannot be completely eliminated. We have examined a full layer of Co atoms (1 ML, in total 9 Co atoms) deposited on the Co(100) surface and this is shown in Fig. 11(a). The initial surface Co atoms become trench Co atoms and the deposited Co atoms become new surface Co atoms. From our previous thermodynamic study on NH_x-terminated Co surfaces, NH_2 prefers a surface bridge site and NH prefers a trench bridge site.[31] With this in mind, we have performed calculations of surface rearrangement on the NH_x-terminated Co(100) surface with a full layer of deposited Co atoms. The relaxed structure is shown in Fig. 11(b). This surface NH_x rearrangement is exothermic with a negative energy gain at the value of −0.48 eV. After rearrangement, NH_2 binds to surface bridge sites.

From the experimentally reported XRD results,[46,47] three representative surface facets, including both Co(001) and Co (100), are detected and show clear peaks, which is why we use these surface terminations in our work. Our DFT models have simplified the deposition process and conditions and focus on specific aspects of the chemistry of deposition. It is worth noting that ALD growth of Co thin films tends to be amorphous or polycrystalline and after annealing, the orientations of the deposited Co thin film will show up.

4.2 Regeneration of surface NH_x terminations at the post-plasma stage

We analyse the process of the chemistry with the plasma species in two steps, namely (1) removal of surface Cp ligands

Table 2 The computed charge transfer with Bader charge analysis, q(Bader) − q(valence), for the elimination of surface NH_x species on a 3CoCp fragments terminated Co(001) surface and an NH_x-terminated Co(100) surface. Noted that the Cp ligands are eliminated prior to surface NH species on Co(001) surface

	1st NH_x removal NH_3	2nd NH_x removal NH_3	3rd NH_x removal NH_3	4th NH_x removal NH_3	5th NH_x removal NH_3	6th NH_x removal NH_3	7th NH_x removal NH_3	8th NH_x removal NH_3	9th NH_x removal NH_3
Co(001)	$-0.08e^-$	$-0.11e^-$	$-0.10e^-$	$-0.09e^-$	$-0.10e^-$	$-0.10e^-$	$-0.07e^-$	$-0.08e^-$	$-0.08e^-$
Co(100)	$-0.05e^-$	$-0.06e^-$	$-0.06e^-$	$-0.08e^-$	$-0.11e^-$	$-0.13e^-$	—	—	—

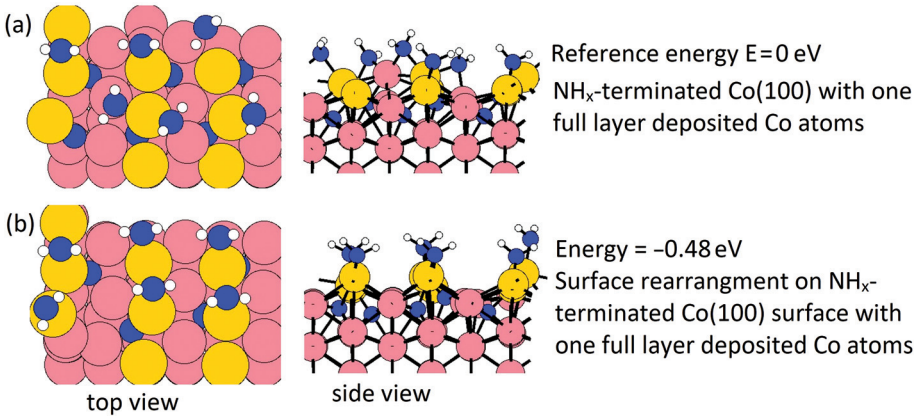

Fig. 11 The top view and side view of (a) relaxed original structure, and (b) structure after surface NH_x rearrangement on NH_x-terminated Co(100) with one full layer of deposited Co atoms. Carbon, nitrogen, and hydrogen atoms are presented in grey, blue, and white colours. Substrates Co and Co from $CoCp_2$ are represented by pink and red spheres, respectively.

and surface NH_x species and (2) regeneration of surface NH_x termination at post-plasma stage.

For modelling the chemistry with plasma species, the first step is to investigate the removal of any remaining Cp ligands and surface NH_x species with plasma-generated radicals $^{\bullet}H$, $^{\bullet}NH$, $^{\bullet}NH_2$, and $^{\bullet}N$. On the Co(001) surface, our calculations show that the Cp ligands and surface NH_x species will be completely removed, resulting in deposited Co atoms on the Co (001) surface at a coverage of 3.03 Co nm^{-2}.

In the second step, we then model the addition of NH_x radicals to the surface obtained from the first step. If we consider the next ALD cycle, at the post-plasma stage, the metal surface is supposed to be terminated with NH_x species before the next metal precursor half-reaction, analogous to the regeneration of hydroxyl groups in thermal- or plasma-assisted metal oxide ALD.[48,49] To explore how this surface can form, we have performed MD calculations at 600 K for the interaction of $^{\bullet}NH$ radicals with the Co(001) surface, where Co atoms were deposited at a coverage of 3.03 Co nm^{-2} and the original surface NH species were eliminated as ammonia. Two coverages of $^{\bullet}NH$ radicals are explored, *i.e.* 0.67 ML (in total 6 NH) and 0.89 ML (in total 8 NH) on a (3 × 3) supercell (1 ML corresponds to 9 NH radicals). The time step is 1.5 fs with a simulation time of 2.25 ps in the NVT ensemble. The structures at the two coverage of NH radicals after MD calculations are shown in Fig. 12.

From these simulations, the Co(001) surface is covered with NH terminations at a coverage of 0.44 ML (4 NH on the surface). This coverage is slightly lower than the determined stable coverage of NH terminations on Co(001) surface from our previous study,[31] which is 0.56 ML (5 NH on the surface). At an initial higher coverage of 0.89 ML NH, we observe the formation of surface-bound NH and NH_2 species, as well as surface-bound H species and N species, which form as a result of the dissociation of NH radicals under these simulation conditions. We can infer that at the post-plasma stage, NH radicals contribute to the formation of the NH_x-terminations on the metal surface, which then contributes in the Cp ligand

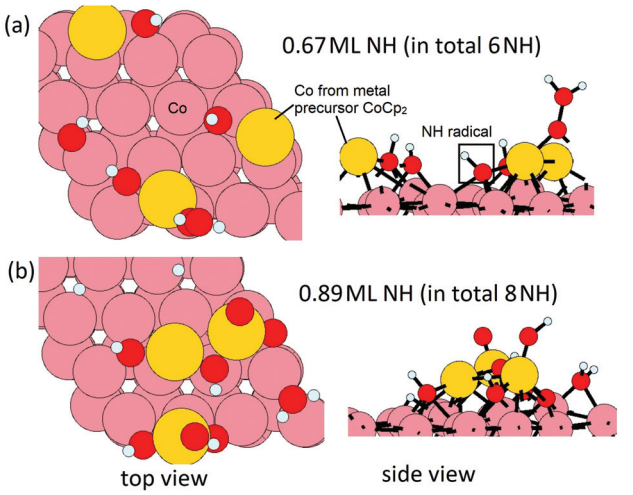

Fig. 12 The configurations of the structures after MD calculations on the Co(001) surface with NH radicals at the coverage of (a) 0.67 ML, and (b) 0.89 ML. Carbon, nitrogen, and hydrogen atoms are presented in grey, blue, and white colours. Substrates Co and Co from $CoCp_2$ are represented by pink and yellow spheres, respectively. Plasma-generated N and H radicals are represented by red and light blue spheres, respectively.

elimination in the next metal precursor pulse. Hydrogen alone cannot produce the reactive NH species; although N_2 alone would promote Cp ligand elimination *via* pyridine formation, these $^{\bullet}N$ radicals cannot produce reactive NH surface termination. Thus, the plasma deposition of Co requires both hydrogen and nitrogen/ammonia plasma.

Then, we perform MD calculations at 600 K to explore how NH_x terminations are formed on the Co(100) surface at the post-plasma stage. The Co(100) surface after NH_x rearrangement (Fig. 11(b)) is chosen to be the substrate. The coverage of NH radicals is 0.67 ML (in total 6 NH), which was previously determined as the saturation coverage of trench NH species at

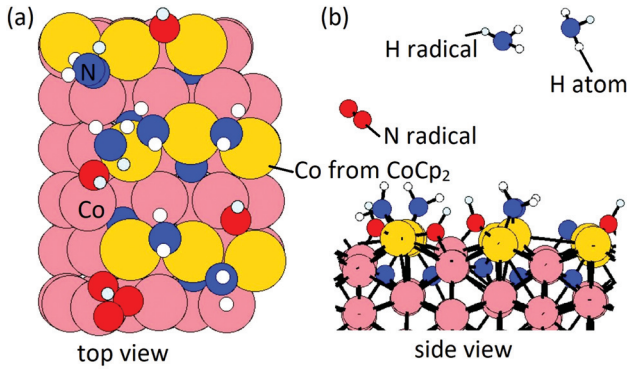

Fig. 13 The configurations of the (a) initial structure, and (b) final structure for MD calculations on the structure after surface rearrangement and NH radicals. Carbon, nitrogen, and hydrogen atoms are presented in grey, blue, and white colours. Substrates Co and Co from $CoCp_2$ are represented by pink and yellow spheres, respectively. Plasma-generated N and H radicals are represented by red and light blue spheres, respectively.

the ALD deposition temperature.[31] The time step is 1.5 fs with a simulation time of 2.25 ps with the NVT (or canonical) ensemble. The initial structure and final structure are shown in Fig. 13. By-products NH_3 and N_2 are formed and released, resulting in surface terminations of surface-bound N, surface-bound NH_2, and trench NH species. The original trench N atoms are now incorporated into the subsurface layer. One full layer of Co atoms is deposited and the terminations after the post-plasma stage are NH_x-terminations with 4 NH_2 + 4 NH on the Co(100) surface. This coverage is slightly lower than the determined stable coverage of mixed terminations on the Co(100) surface from our previous study,[31] which is 6 NH + 6 NH_2 on the surface.

It is noted that the trench N species are present throughout the deposition process and cannot be removed completely in either the metal precursor or plasma cycle. We can infer that the N impurities exists with the possibility of formation of Co_xN. This is consistent with the reported nitrogen incorporation into deposited Co thin films and cobalt nitride using $CoCp_2$ and NH_3 plasma.[30,45] At temperatures of 533 K and below, the deposited thin films consist primarily of Co_2N. At the higher temperature at 573 K, the Co_xN is a mixture of Co_3N and Co. Finally, if the temperature is up to 623 K, the deposited thin film is nominally pure Co, which is due to the decomposition of cobalt nitride.[30] Detailed studies are needed to unravel the formation of surface cobalt nitride and removal of these N species, which is out of the scope of this work.

4.3 Source of O, C, and N impurities during PE-ALD of Co using $CoCp_2$ and N-plasma

In the experimental work of Vos *et al.*,[27] the XPS measurements showed that when using NH_3 or mixture of H_2 and N_2 as the plasma source, the deposited Co thin film has minimal amounts of O, C, and N and no other impurities were detected. In contrast, in the ABC-type ALD process, where N_2 and H_2 are pulsed into the chamber separately, the deposited Co thin film shows significant amounts of O, C, and N impurities. The O incorporation is likely due to the dissociation of background species, such as H_2O, in the plasma during film growth. The detailed analysis of O incorporation is excluded in our work and is out of the scope of this paper.

We can attribute the dramatically increased contents of C impurities in the separate N_2/H_2 plasma process to the lack of active NH_x species and a preference for the dissociation of the Cp ligand from the metal precursor $CoCp_2$. When using NH_3 or a mixture of N_2 and H_2 as the plasma source, the plasma-generated NH_x species help to form NH_x terminations on the Co surface[31] and in the metal precursor pulse these NH_x terminations eliminate intact Cp ligands as CpH *via* H transfer from the surface.[32] But, when using separated pulsed N_2 and H_2 as the plasma source, the lack of active NH_x surface species does not allow this mechanism in the metal precursor pulse and dissociation of Cp can be promoted, which results in high carbon impurity content in the deposited Co thin film.

In addition to our work,[32] the present results reveal that in the plasma pulse the elimination of Cp ligands can proceed *via* H transfer and CpH formation and desorption or by pyridine formation, both of which prevent undesired C incorporation. Recognising that while our DFT model has unavoidably simplified the whole deposition process, our results are consistent with the conclusions of Vos *et al.*[27] that the C impurity of the Co thin film can be attributed to avoiding Cp ligand decomposition and the metal precursor reacts with active surface NH_x species, desorbing CpH from the metal surface.

For the N impurities, this work highlights that at the plasma pulse, the N species cannot be completely removed with plasma-generated radicals $^{\bullet}H$, $^{\bullet}NH$, and $^{\bullet}NH_2$ and thus becomes the source of N impurities in the deposited Co thin film. On the Co(100) surface, the removal of surface NH_2 species as ammonia is endothermic and the energy cost of NH_3 desorption on Co(100) surface is around 1.2 eV at each desorption step. However, on Co(100), the plasma-generated H radicals react with trench N species to form stable NH species, which are then available for the next hydrogen transfer step in the next metal precursor pulse. After a full layer of deposited Co on the along [100] direction, due to the zigzag structure, the original substrate surface Co atoms become new trench Co atoms, and the new deposited full layer of Co becomes the new surface Co atoms. These new trench and surface Co atoms are then covered with NH_x terminations to perform the next deposition cycle. The N impurities are due to the difficulty and high energy cost of removal of those N species bonding to the original trench Co atoms.

5. Conclusions

We have presented a detailed first principles study of the chemistry of the plasma pulse in hydrogen/nitrogen plasma-enhanced ALD of Co metal. We begin with a surface after the metal precursor pulse, with the CoCp fragment-terminated

Co(001) surface at a coverage of 3.03 CoCp nm^{-2} and an NH_x-terminated Co(100) surface with deposited Co atoms at a coverage of 3.33 Co nm^{-2}. This work focuses on the reaction mechanism in the plasma cycle of plasma radicals and Co(001) and Co(100) surfaces terminated with the Cp ligand (if any) and NH_x species on the atomic scale.

On the Co(001) surface, the preferred reaction mechanism is that the Cp ligand is eliminated prior to surface NH_x species *via* pyridine formation and desorption with plasma generated $^{\bullet}N$ radicals. Bader charge analysis indicates that for the ammonia desorption step, the Cp ligand eliminated prior to NH_x elimination has less transferred charge between NH_3 and substrate Co, compared to the Cp ligand present throughout. The surface NH species and N species are eliminated *via* intermediate NH formation, NH_2 formation, by-product NH_3 formation and desorption. The reactions of Cp ligand removal and subsequent NH_x removal are overall exothermic, which are completely eliminated on the Co(001) surface, resulting in deposition of Co atoms on the (001) surface at a coverage of 3.03 Co nm^{-2}.

There is a different behaviour on the Co(100) surface. The surface NH_2 species cannot be completely removed with $^{\bullet}H$ radicals *via* NH_3 formation and desorption due to an overall endothermic reaction energy. Instead, $^{\bullet}H$ radicals will contribute to re-form the trench NH species with computed negative reaction energies. When a full layer of Co atoms is deposited on the Co(100) surface, due to its unique zigzag structure, the original surface Co atoms become trench Co and the deposited Co atoms occupy the surface site. However, these trench N species are present throughout the deposition process and result in the formation of Co_xN and cannot be removed completely under the conditions of our simulations. This indicates that the plasma species act as the source of N impurities in the deposited Co thin films.

At the post-plasma stage, MD simulations at 600 K show that NH radicals play an important role in the regeneration of NH_x terminations on Co(001) and (100) surfaces, which are then ready for the next metal precursor half-cycle. For Cp-based metal precursors, NH_x species are required to deposit Co thin films with high purity and low resistivity, which explains why NH_3 plasma or a mixture of N_2 and H_2 plasma are the plasma sources that work best, rather than H_2 plasma or N_2 plasma alone.

Conflicts of interest

There are no conflicts to declare.

Acknowledgements

We acknowledge the generous support from Science Foundation Ireland (SFI) through the SFI-NSFC Partnership program, Grant Number 17/NSFC/5279, NITRALD and the National Natural Science Foundation of China, Grant number 51861135105. Computing resources have been generously supported by Science Foundation Ireland at Tyndall and through the SFI/HEA-funded Irish Centre for High End Computing (http://www.ichec.ie). J. L. acknowledges that part of the results of this research have been achieved using the DECI resource BEM cluster based in Poland at Wroclaw Centre for Networking and Supercomputing with support from the PRACE (https://prace-ri.eu/hpc-access/deci-access/).

References

1 K. Tu, Recent Advances on Electromigration in Very-Large-Scale-Integration of Interconnects, *J. Appl. Phys.*, 2003, **94**, 5451–5473.
2 S. Kondati Natarajan, C.-L. Nies and M. Nolan, Ru passivated and Ru doped ε-TaN surfaces as a combined barrier and liner material for copper interconnects: a first principles study, *J. Mater. Chem. C*, 2019, **7**(26), 7959–7973.
3 D. V. Greenslit and E. Eisenbraun, Characterization of Ultrathin PEALD-Grown RuCo Films for Diffusion Barrier and Copper Direct-Plate Applications, *ECS Trans.*, 2011, **35**, 17–24.
4 T. Chakraborty and E. T. Eisenbraun, Microstructure Analysis of Plasma Enhanced Atomic Layer Deposition-Grown Mixed-Phase RuTaN Barrier for Seedless Copper Electrodeposition, *J. Vac. Sci. Technol., A*, 2012, **30**, 020604.
5 V. Miikkulainen, M. Leskelä, M. Ritala and R. L. Puurunen, Crystallinity of Inorganic Films Grown by Atomic Layer Deposition: Overview and General Trends, *J. Appl. Phys.*, 2013, **113**, 021301.
6 R. W. Johnson, A. Hultqvist and S. F. Bent, A Brief Review of Atomic Layer Deposition: From Fundamentals to Applications, *Mater. Today*, 2014, **17**, 236–246.
7 A. E. Kaloyeros, Y. Pan, J. Goff and B. Arkles, Review—Cobalt Thin Films: Trends in Processing Technologies and Emerging Applications, *ECS J. Solid State Sci. Technol.*, 2019, **8**, P119–P152.
8 S. M. George, Atomic Layer Deposition: An Overview, *Chem. Rev.*, 2009, **110**, 111–131.
9 H. Profijt, S. Potts, M. Van de Sanden and W. Kessels, Plasma-Assisted Atomic Layer Deposition: Basics, Opportunities, and Challenges, *J. Vac. Sci. Technol., A*, 2011, **29**, 050801.
10 P. O. Oviroh, R. Akbarzadeh, D. Pan, R. A. M. Coetzee and T. C. Jen, New Development of Atomic Layer Deposition: Processes, Methods and Applications, *Sci. Technol. Adv. Mater.*, 2019, **20**, 465–496.
11 H. Kim, Atomic Layer Deposition of Mmetal and Nitride Thin Films: Current Research Efforts and Applications for Semiconductor Device Processing, *J. Vac. Sci. Technol., B: Microelectron. Nanometer Struct.–Process., Meas., Phenom.*, 2003, **21**, 2231–2261.
12 T. J. Knisley, L. C. Kalutarage and C. H. Winter, Precursors and Chemistry for The Atomic Layer Deposition of Metallic

First Row Transition Metal Films, *Coord. Chem. Rev.*, 2013, **257**, 3222–3231.
13 H. Kim, Area Selective Atomic Layer Deposition of Cobalt Thin Films, *ECS Trans.*, 2008, **16**, 219–225.
14 B. S. Lim, A. Rahtu and R. G. Gordon, Atomic Layer Deposition of Transition Metals, *Nat. Mater.*, 2003, **2**, 749–754.
15 J.-M. Kim, C. Lansalot, C. Dussarrat, J. Gatineau and H. Kim, Plasma-enhanced atomic layer deposition of cobalt using cyclopentadienyl isopropyl acetamidinato-cobalt as a precursor, *Jpn. J. Appl. Phys.*, 2010, **49**, 05FA10.
16 K. Kim, K. Lee, S. Han, W. Jeong and H. Jeon, Characteristics of Cobalt Thin Films Deposited by Remote Plasma ALD Method with Dicobalt Octacarbonyl, *J. Electrochem. Soc.*, 2007, **154**, H177–H181.
17 H. Kim, High-Quality Cobalt Thin Films by Plasma-Enhanced Atomic Layer Deposition, *Electrochem. Solid-State Lett.*, 2006, **9**, G323–G325.
18 R. L. Puurunen, Surface Chemistry of Atomic Layer Deposition: A Case Study for The Trimethylaluminum/Water Process, *J. Appl. Phys.*, 2005, **97**, 121301.
19 S. Elliott, G. Scarel, C. Wiemer, M. Fanciulli and G. Pavia, Ozone-Based Atomic Layer Deposition of Alumina from TMA: Growth, Morphology, and Reaction Mechanism, *Chem. Mater.*, 2006, **18**, 3764–3773.
20 T. Weckman and K. Laasonen, First Principles Study of The Atomic Layer Deposition of Alumina by TMA–H_2O-Process, *Phys. Chem. Chem. Phys.*, 2015, **17**, 17322–17334.
21 T. Weckman and K. Laasonen, Atomic Layer Deposition of Zinc Oxide: Diethyl Zinc Reactions and Surface Saturation from First-Principles, *J. Phys. Chem. C*, 2016, **120**(38), 21460–21471.
22 S.-J. Lee, S.-H. Kim, M. Saito, K. Suzuki, S. Nabeya, J. Lee, S. Kim, S. Yeom and D.-J. Lee, Plasma-Free Atomic Layer Deposition of Ru Thin Films Using H_2 Molecules as A Nonoxidizing Reactant, *J. Vac. Sci. Technol., A*, 2016, **34**(3), 031509.
23 B. Zhu, Z.-J. Ding, X. Wu, W.-J. Liu, D. W. Zhang and S.-J. Ding, Plasma-Enhanced Atomic Layer Deposition of Cobalt Films Using $Co(EtCp)_2$ as A Metal Precursor, *Nanoscale Res. Lett.*, 2019, **14**, 76.
24 H. Kim and I.-K. Oh, Review of plasma-enhanced atomic layer deposition: Technical enabler of nanoscale device fabrication, *Jpn. J. Appl. Phys.*, 2014, **53**(3S2), 03DA01.
25 S. Rossnagel, A. Sherman and F. Turner, Plasma-enhanced atomic layer deposition of Ta and Ti for interconnect diffusion barriers, *J. Vac. Sci. Technol., B: Microelectron. Nanometer Struct.–Process., Meas., Phenom.*, 2000, **18**, 2016–2020.
26 J. Yoon, D. Kim, T. Cheon, S.-H. Kim and H. Kim, Atomic Layer Deposition of Co Using N_2/H_2 Plasma as A Reactant, *J. Electrochem. Soc.*, 2011, **158**, H1179–H1182.
27 M. F. J. Vos, G. van Straaten, W. E. Kessels and A. J. Mackus, Atomic Layer Deposition of Cobalt Using H_2-, N_2-, and NH_3-Based Plasmas: On the Role of the Co-reactant, *J. Phys. Chem. C*, 2018, **122**, 22519–22529.
28 M. Nolan and S. D. Elliott, Competing Mechanisms in Atomic Layer Deposition of Er_2O_3 versus La_2O_3 from Cyclopentadienyl Precursors, *Chem. Mater.*, 2010, **22**, 117–129.
29 V. R. Rai, V. Vandalon and S. Agarwal, Surface Reaction Mechanisms During Ozone and Oxygen Plasma Assisted Atomic Layer Deposition of Aluminum Oxide, *Langmuir*, 2010, **26**, 13732–13735.
30 G. van Straaten, R. Deckers, M. F. Vos, W. M. Kessels and M. Creatore, Plasma-Enhanced Atomic Layer Deposition of Cobalt and Cobalt Nitride: What Controls the Incorporation of Nitrogen?, *J. Phys. Chem. C*, 2020, **124**, 22046–22054.
31 J. Liu and M. Nolan, Coverage and Stability of NHx-Terminated Cobalt and Ruthenium Surfaces: A First-Principles Investigation, *J. Phys. Chem. C*, 2019, **123**, 25166–25175.
32 J. Liu, H. Lu, D. W. Zhang and M. Nolan, Reaction Mechanism of the Metal Precursor Pulse in Plasma-Enhanced Atomic Layer Deposition of Cobalt and the Role of Surface Facets, *J. Phys. Chem. C*, 2020, **124**, 11990–12000.
33 M. Sode, W. Jacob, T. Schwarz-Selinger and H. Kersten, Measurement and modeling of neutral, radical, and ion densities in H2-N2-Ar plasmas, *J. Appl. Phys.*, 2015, **117**, 083303.
34 H. Shimizu, K. Sakoda, T. Momose, M. Koshi and Y. Shimogaki, Hot-wire-assisted atomic layer deposition of a high quality cobalt film using cobaltocene: Elementary reaction analysis on NH x radical formation, *J. Vac. Sci. Technol., A*, 2012, **30**(1), 01A144.
35 G. Kresse and D. Joubert, From Ultrasoft Pseudopotentials to The Projector Augmented-wave Method, *Phys. Rev. B: Condens. Matter Mater. Phys.*, 1999, **59**, 1758–1775.
36 G. Kresse and J. Hafner, Ab initio molecular-dynamics simulation of the liquid-metal–amorphous-semiconductor transition in germanium, *Phys. Rev. B: Condens. Matter Mater. Phys.*, 1994, **49**, 14251.
37 J. P. Perdew, J. A. Chevary, S. H. Vosko, K. A. Jackson, M. R. Pederson, D. J. Singh and C. Fiolhais, Atoms, Molecules, Solids, and Surfaces: Applications of The Generalized Gradient Approximation for Exchange and Correlation, *Phys. Rev. B: Condens. Matter Mater. Phys.*, 1992, **46**, 6671–6687.
38 J. P. Perdew, K. Burke and M. Ernzerhof, Generalized Gradient Approximation Made Simple, *Phys. Rev. Lett.*, 1996, **77**, 3865–3868.
39 H. J. Monkhorst and J. D. Pack, Special Points for Brillouin-zone Integrations, *Phys. Rev. B: Solid State*, 1976, **13**, 5188–5192.
40 C. Yoo, H. Cynn, P. Söderlind and V. Iota, New β (fcc)-Cobalt to 210 GPa, *Phys. Rev. Lett.*, 2000, **84**, 4132.
41 Y. Maimaiti and S. D. Elliott, Precursor Adsorption on Copper Surfaces as the First Step during the Deposition of Copper: A Density Functional Study with van der Waals Correction, *J. Phys. Chem. C*, 2015, **119**, 9375–9385.

42 M. Yu and D. R. Trinkle, Accurate and efficient algorithm for Bader charge integration, *J. Chem. Phys.*, 2011, **134**, 064111.
43 W. Tang, E. Sanville and G. Henkelman, A grid-based Bader analysis algorithm without lattice bias, *J. Phys.: Condens. Matter*, 2009, **21**, 084204.
44 M. Shirazi and S. D. Elliott, Cooperation between adsorbates accounts for the activation of atomic layer deposition reactions, *Nanoscale*, 2015, **7**, 6311–6318.
45 J. Reif, M. Knaut, S. Killge, F. Winkler, M. Albert and J. W. Bartha, In Vacuo Studies on Plasma-Enhanced Atomic Layer Deposition of Cobalt Thin Films, *J. Vac. Sci. Technol., A*, 2020, **38**, 012405.
46 N. Arora and B. R. Jagirdar, Carbonization of solvent and capping agent based enhancement in the stabilization of cobalt nanoparticles and their magnetic study, *J. Mater. Chem.*, 2012, **22**, 20671–20679.
47 Q. Meng, S. Guo, X. Zhao and S. Veintemillas-Verdaguer, Bulk metastable cobalt in fcc crystal structure, *J. Alloys Compd.*, 2013, **580**, 187–190.
48 J. Van Hemmen, S. Heil, J. Klootwijk, F. Roozeboom, C. Hodson, M. Van de Sanden and W. Kessels, Plasma and Thermal ALD of Al2O3 in a Commercial 200 mm ALD Reactor, *J. Electrochem. Soc.*, 2007, **154**, G165.
49 G. N. Fomengia, M. Nolan and S. D. Elliott, First principles mechanistic study of self-limiting oxidative adsorption of remote oxygen plasma during the atomic layer deposition of alumina, *Phys. Chem. Chem. Phys.*, 2018, **20**, 22783–22795.